Supplementary Material DR2012111

Rapid response of Helheim Glacier, south-east Greenland to early Holocene climate warming

Anna L.C. Hughes*, Eleanor Rainsley, Tavi Murray, Christopher J. Fogwill, Christoph Schnabel, Sheng Xu.
*Email: a.hughes@swansea.ac.uk

Methods

Field sampling

The deglaciated coastal zone of SE Greenland is virtually devoid of depositional markers of ice margin retreat and in situ terrestrial cosmogenic nuclide (^{10}Be) exposure dating is one of the few means to constrain a glacial retreat chronology and develop our understanding of long-term outlet glacier change. Rock samples were collected during field campaigns to Sermilik Fjord, SE Greenland during July 2009 and 2010. A paired sampling strategy was employed taking samples from rounded erratic cobbles or boulders perched on polished striated streamlined bedrock surfaces at exposed sites along the fjord walls. Sample locations were reached by boat and on foot; favourable ice conditions and numerous possible landing points enabled selection of sites spanning the full length of Sermilik Fjord (Fig. DR1). Streamlined bedrock surfaces and subsamples of upper surfaces (upper 5-7 cm) of boulder and large cobble erratics were removed manually using a 4 lb lump hammer and chisel. In other cases whole erratic cobbles were collected. In each case approximately 2 kg rock was obtained per sample. Samples were obtained from low elevations but above the local marine limit (identified by the lowest level of glacial erratic cobbles and boulders) where possible, to capture the most recent occupation by ice at each site and avoid the likelihood of nuclide inheritance (Briner et al., 2009). The marine limit was recorded as at ~55 m close to the fjord mouth by Roberts et al. (2008), but the presence of erratic cobbles at ~40 m suggests that the marine limit at the mouth of Helheimfjord was slightly lower here (Table DR1). Sample SF-09-01 was taken from a site close to the mouth of the fjord below the marine limit (37 m), but is unlikely to have been submerged for a long period of time if rebound was quick. Care was taken to avoid hollows and other potential areas of snow accumulation and/or drifting. Sample location and elevation were recorded using handheld GPS receivers (±10 m). Topographic shielding was measured using a sighting clinometer. Sample and location details are recorded in Table DR1.

Analytical methods

Samples were reduced to pure quartz at the University of Exeter Cosmogenic Nuclide Laboratory and the NERC Cosmogenic Isotope Analysis Facility (CIAF) at the Scottish Universities Environmental Research Centre (SUERC) following standard procedures (e.g. Stone, 2004; Kohl and Nishiizumi, 1992; Ivy Ochs, 1996). Samples were run in three batches (n = 5, n =3 and n = 4), the first two at the CIAF and the third at the University of Exeter. ^{10}Be ratios were measured by the AMS laboratory at SUERC (Xu et al., 2010). Measurements were normalised to the NIST SRM-4325 Be standard material with a revised nominal ^{10}Be/^{9}Be ratio of 2.79 x 10^{-11}(Nishiizumi et al., 2007). Samples were corrected for the ^{10}Be/^{9}Be ratio of their

associated blanks (n=5, n=4 and n = 1). Blanks were spiked with 195-245 μg ^{9}Be carrier (CIAF) and 253-254 μg ^{9}Be carrier (University of Exeter). The corresponding combined process and carrier blanks ratios range between 3.6–5.5 x 10^{-15}. Blank corrections ranged between 3-8 % of the measured ^{10}Be/^{9}Be ratio. Sample and blank ^{10}Be/^{9}Be analytical uncertainties and a 2.5% carrier addition uncertainty propagated into the 1σ analytical uncertainty for nuclide concentrations.

Age determinations

Exposure ages were calculated using a version of the CRONUS-Earth online age calculator (June 2009) (http://hess.ess.washington.edu/math/al_be_v22/Age_input_NENA_calib.html), which uses the recently revised ^{10}Be half-life (1.387 Ma) (Chmeleff et al., 2010; Korschinek et al., 2010) and Be isotope ratio standardization of Nishiizumi et al. (2007), and implementing the regional ^{10}Be production rate calibration dataset for NE America (Balco et al. 2009). Exposure ages are reported based on the Lal/Stone (Lal, 1991; Stone, 2000) scaling model; using the same calibration data set, ages differ by 1-4% depending on the choice of alternative scaling model (Table DR2), but the choice does not affect the estimated rate of retreat. The calculator uses sample thickness and density to standardise nuclide concentrations to the rock surface. We used an assumed density of 2.62 g cm^{-3} (equivalent to the density of pure quartz). Samples from adjacent Torqulertivit Imiat Valley (TIV) with similar geological provenance had densities ranging from 2.62 to 2.74 g cm^{-3} (Roberts et al. 2008) and so we consider this assumption reasonable; using the calculated density of the most dense sample increases of exposure ages by ~0.3%. We include no correction for periodic snow cover or for rock-surface erosion, both of which are assumed to be negligible, the former due to our choice of exposed sites not conducive to snow accumulation and/or drifting. An erosion rate of 2 x 10^{-4} cm yr^{-1} (after André, 2002) increases ages by ~2% (Table DR1). No correction for post-glacial isotopic uplift has been applied, although a local relative sea level curve is available from adjacent Ammassalik Fjord, ~20 km to the east of Sermilik Fjord (Long et al., 2008), as we expect any additional age uncertainty due to this to be similarly small (Goehring et al. in press; Kelly et al. 2008). In similar settings elsewhere in Greenland and the Arctic, most of the rebound has occurred by the time the ice is at the heads of the fjords, hence any effect is low and more importantly, the exposure history of each sample is integrated over the whole Holocene, further reducing the effect. Kelly et al. (2008) estimated 2-3% increase in ages for Early Holocene-lateglacial samples from Scoresby Sund due to ~134 m uplift.

Choice of production rate model and scaling is often a pragmatic one and is an ongoing subject of debate. For this reason, and to facilitate comparison with other datasets and earlier work, we also report age results using the other four most commonly used scaling schemes and the CRONUS-global production rate model (Tables DR2 and DR3). The latter ages were generated using the original CRONUS-Earth calculator Version 2.2 March 2009 (http://hess.ess.washington.edu/math/al_be_v22/al_be_multiple_v22.php) (Balco et al. 2008). If the CRONUS-global production rate model is implemented without any calibration, ages are up to 12% younger depending on the scaling scheme used. On the Lal/Stone (Lal, 1991; Stone, 2000) scheme, as reported in this paper, ages are ~12 % younger using the CRONUS-global rather than a calibrated production

rate model. Note that the rate of retreat is not dependent on the choice of production rate and the timing of retreat remains the earliest Holocene. We consider the ages based on the regional production rate calibration dataset for NE America to be more reliable than those based on the CRONUS-global production rate. Unlike the current global calibration dataset the NE American model is not dominated by high altitude, low latitude sites (Balco et al. 2009). At our low altitude, high latitude location this distinction is not trivial. Validation of the use of the NE American calibration data was demonstrated at a similar low altitude, high altitude site, Jakobshaven Isbrae in West Greenland, by comparison with ages derived from radiocarbon analysis (Young et al., 2011). Unfortunately there is not a wealth of independently calculated dates on which to corroborate ages in SE Greenland. However, two radiocarbon dates of 8,980±130 and 9,890±110 ^{14}C yr BP (9.9-10.3 cal. ka BP and 11.2-11.4 cal. ka; Jakobsen et al., 2008) from basal organic sediments in two lakes on the western shore of Sermilik Fjord, north of Mittivakkat Glacier, support the older ages. Using the NE American calibration data also improves the precision of the ages and reduces the differences between different scaling schemes (Tables DR2 and DR3). Recent studies from southern Norway and west Greenland indicate that a lower production rate is more realistic for these sites and that use of the CRONUS-global rate will underestimate surface ages (Goehring et al. 2011; Briner et al. in press). This further demonstrates that use of the NE American rate is appropriate in this case.

For comparison, four previously published ages from the lower TIV were recalculated using the same scaling and production rate as new ages reported in this paper (Table DR4). Two radiocarbon ages from two lakes north of Mittivakkat Glacier (Jakobsen et al. 2008) were recalibrated using Calib v.6.0.1 (Stuiver and Reimer, 1993) and INTCAL09 (Reimer et al. 2009) and are reported as 1σ ranges in the text.

Discussion: erratic vs. bedrock ages

To examine the relationship of bedrock and erratic ages we generated relative probability plots of the ages (Figs. DR2 and DR3). These plots show, that although the all ages overlap within 2 s.d. error, the bedrock ages are consistently older than the erratic ages and some of the bedrock ages likely contain isotopic inheritance due to insufficient erosion. We therefore have based our main conclusions in the paper solely on the erratic ages. These ages show remarkable consistency. From the relative probability plots (Fig. DR3), the youngest erratic age at the mouth of Helheimfjord could potentially reflect a minor slowdown in retreat rate as Helheim, Fenris and Midgaard glaciers separated north of the island, but more data is required to confirm this.

The finding of inheritance in the bedrock samples from Sermilik Fjord is interesting, as paired ^{26}Al/^{10}Be measurements indicated a simple erosion and exposure history for bedrock samples in the TIV on the west side of Sermilik Fjord (Roberts et al. 2008), with the lowest elevation sample (78 m) yielding an age similar to our mouth sample (12.6 ± 1.1 ka B.P.). The similarity of the new data with four existing ages from the TIV (Roberts et al., 2008) suggests that initial separation of the land-terminating tributary glacier occurred

contemporaneously with deglaciation of Sermilik Fjord. The retreat trajectories of the two glaciers after this point appear to have diverged; moraines along the TIV indicate multiple standstills of the ice front during deglaciation (Roberts et al., 2008) whereas there is no landform evidence for periodic stabilization of the glacier occupying Sermilik Fjord.

Table DR1 Sample details and ^{10}Be surface exposure ages from Sermilik Fjord, SE Greenland.

Sample Name	AMS id	Latitude °N	Longitude °W	Sample type	Lithology	Elevation (m asl*)	Thickness (cm)	Shielding correction	Thickness scaling factor#	Mass (g)	Be carrier added (ml)	^{10}Be/^{9}Be ratio† (x 10^{-14})	^{10}Be (x 10^{4} atoms/g)§	Sigma ^{10}Be (x 10^{3} atoms/g)	Internal uncertainty (yr)	Exposure age (zero erosion) (kyr)**	Exposure age (0.0002 cm/yr erosion) (kyr)**
Sermilik Fjord mouth, east side (2 km from fjord mouth)																	
SF-09-01	b4781	65.6338	37.9482	Bedrock	Gneiss/schist	37	5	0.9990	0.9602	30.1	0.2625	9.7790	5.514	1.25	290	**12.7 ± 0.7**	13.0 ± 0.7
Mid-Sermilik Fjord, west side (27 km from Sermilik Fjord mouth)																	
SF-09-62	b4483	65.8570	38.0061	Erratic cobble	Granodiorite	112	7	0.9902	0.9448	30.2	0.205	9.8890	4.862	1.68	370	**10.7 ± 0.6**	10.9 ± 0.7
SF-09-63	b4426	65.8569	38.0060	Erratic cobble	Granodiorite	110	7	0.9900	0.9448	18.4	0.181	6.9852	4.983	2.56	566	**11.0 ± 0.8**	11.2 ± 0.8
SF-09-64	b4303	65.8570	38.0062	Streamlined bedrock	Banded gneiss	116	7.5	0.9898	0.9410	13.4	0.2266	4.575	5.596	2.61	576	**12.3 ± 0.8**	12.6 ± 0.9
Mid-Sermilik Fjord, east side (57 km from Sermilik Fjord mouth)																	
SF-09-53	b4482	66.0599	37.7049	Streamlined bedrock	Banded gneiss	110	8.5	0.9939	0.9335	24.9	0.2145	10.840	5.213	1.45	324	**11.6 ± 0.6**	11.8 ± 0.7
SF-09-54	b4300	66.0599	37.7049	Erratic cobble	Banded gneiss	111	10	0.9939	0.9224	22.2	0.2266	6.535	4.822	1.70	384	**10.9 ± 0.6**	11.0 ± 0.7
SF-09-55	b4301	66.0599	37.7049	Erratic cobble	Banded gneiss	110	10	0.9939	0.9224	26.8	0.2266	8.207	5.018	1.84	416	**11.3 ± 0.7**	11.5 ± 0.7
Island at head of Sermilik Fjord, southeast of Helheim Fjord mouth (71 km from Sermilik Fjord mouth)																	
SF-09-29	b4479	66.2262	37.5928	Erratic cobble	Banded gneiss	76	8.5	0.9868	0.9335	24.9	0.1862	8.9171	4.822	1.32	309	**11.2 ± 0.6**	11.5 ± 0.6
SF-09-30	b4480	66.2263	37.5928	Streamlined bedrock	Banded gneiss	77	5	0.9866	0.9602	35.2	0.2218	10.880	4.961	1.52	346	**11.3 ± 0.6**	11.5 ± 0.7
Head of Sermilik Fjord, at junction between Helheim and Fenris Fjords (81 km from Sermilik Fjord mouth)																	
SF-10-01	b4783	66.3185	37.5541	Streamlined bedrock	Banded gneiss	191	5	0.9978	0.9602	30.3	0.2623	10.839	6.056	1.55	310	**12.1 ± 0.7**	12.3 ± 0.7
Helheimfjord mouth, south side (76 km from Sermilik Fjord mouth)																	
SF-09-03	b4787	66.2798	37.7261	Streamlined bedrock	Banded gneiss	40	6.5	0.9946	0.9486	32.3	0.2621	10.058	5.266	2.18	520	**12.5 ± 0.8**	12.8 ± 0.8
SF-09-04	b4782	66.2798	37.7261	Erratic cobble	Banded gneiss	47	8	0.9946	0.9373	32.4	0.2629	8.2166	4.303	1.09	261	**10.3 ± 0.6**	10.4 ± 0.6

Reference datum WGS 84.

*m a.s.l. (metres above sea level). Elevations derived from handheld GPS units, maximum uncertainty ±10 m. No correction applied due to lack of robust regional relative sea level curve (see text).

†Average ^{10}Be/^{9}Be ratios of 3.647 x 10^{-15} , 5.477 x 10^{-15} and 5.162 x 10^{-15} for fully processed blanks was subtracted from the ^{10}Be/^{9}Be ratios of samples SF-09-29, SF-09-30, SF-09-53, SF-09-62, SF-09-63, samples SF-09-54, SF-09-55, SF-09-64, and samples SF-09-01, SF-09-03, SF-09-04 and SF-10-01 respectively.

§Samples are normalized to standard NIST SRM4325 with a certified ratio of 2.79 x 10^{-11} (07KNSTD) (Nishiizumi et al., 2007)

#Thickness correction calculated for an assumed density of 2.62 g/cm^3

**Exposure ages calculated using scaling scheme of Lal/Stone (Lal, 1991; Stone, 2000) using a NE American regionally calibrated production rate model (Balco et al., 2009). No correction for snow cover.

Table DR2 ^{10}Be ages achieved using alternative scaling schemes and calculated using the regionally calibrated North American production rate (Balco et al. 2009). All other parameters kept the same as in Table DR1.

Sample	St (Lal, 1991; Stone, 2000)*	De (Desilets et al., 2006)	Du (Dunai, 2001)	Li (Lifton et al., 2005)	Lm (Time dependent Lal, 1991; Stone, 2000))
SF-09-01	**12.7 ± 0.7**	12.4 ± 0.7	12.3 ± 0.7	12.2 ± 0.7	12.9 ± 0.7
SF-09-03	**12.5 ± 0.8**	12.2 ± 0.8	12.0 ± 0.8	12.0 ± 0.8	12.7 ± 0.8
SF-09-04	**10.3 ± 0.6**	10.0 ± 0.6	9.9 ± 0.5	9.8 ± 0.5	10.4 ± 0.6
SF-09-29	**11.2 ± 0.6**	11.0 ± 0.6	10.9 ± 0.6	10.8 ± 0.6	11.4 ± 0.6
SF-09-30	**11.3 ± 0.6**	11.0 ± 0.6	10.9 ± 0.6	10.8 ± 0.6	11.4 ± 0.7
SF-09-53	**11.6 ± 0.6**	11.4 ± 0.6	11.3 ± 0.6	11.2 ± 0.6	11.8 ± 0.7
SF-09-54	**10.9 ± 0.6**	10.7 ± 0.6	10.5 ± 0.6	10.5 ± 0.6	11.0 ± 0.7
SF-09-55	**11.3 ± 0.7**	11.1 ± 0.7	11.0 ± 0.7	10.9 ± 0.7	11.5 ± 0.7
SF-09-62	**10.7 ± 0.6**	10.5 ± 0.6	10.4 ± 0.6	10.3 ± 0.6	10.8 ± 0.6
SF-09-63	**11.0 ± 0.8**	10.8 ± 0.8	10.7 ± 0.8	10.6 ± 0.8	11.1 ± 0.8
SF-09-64	**12.3 ± 0.8**	12.1 ± 0.8	12.0 ± 0.8	11.9 ± 0.8	12.5 ± 0.8
SF-10-01	**12.1 ± 0.7**	12.0 ± 0.7	11.8 ± 0.7	11.7 ± 0.7	12.3 ± 0.7
Mean (all samples)†	**11.4 ± 0.2**	11.2 ± 0.2	11.0 ± 0.2	11.0 ±0.2	11.6 ±0.2
Mean (erratics)†	**10.8 ± 0.3**	10.6 ± 0.3	10.5 ± 0.3	10.4 ±0.3	11.0 ±0.3
Mean (bedrock)†	**12.0 ± 0.3**	11.8 ± 0.3	11.7 ± 0.3	11.6 ±0.3	12.2 ±0.3

*From Table DR1.
†Error weighted mean and 1 s.d.

Table DR3 ^{10}Be ages derived using alternative scaling schemes calculated using the CRONUS-global production rate. All other parameters kept the same as in Table DR1.

Sample	St (Lal, 1991; Stone 2000)	De (Desilets et al. 2006)	Du (Dunai, 2001)	Li (Lifton et al. 2005)	Lm (Time dependent Lal, 1991; Stone, 2000)
SF-09-01	11.2 ± 1.0	11.7 ± 1.4	11.6 ± 1.4	11.3 ± 1.1	11.5 ± 1.0
SF-09-03	11.0 ± 1.1	11.4 ± 1.4	11.3 ± 1.4	11.1 ± 1.2	11.3 ± 1.1
SF-09-04	9.0 ± 0.8	9.4 ± 1.1	9.3 ± 1.1	9.1 ± 0.8	9.2 ± 0.8
SF-09-29	9.9 ± 0.9	10.3 ± 1.3	10.2 ± 1.2	10.0 ± 1.0	10.1 ± 0.9
SF-09-30	9.9 ± 0.9	10.3 ± 1.3	10.2 ± 1.2	10.0 ± 1.0	10.1 ± 0.9
SF-09-53	10.2 ± 0.9	10.7 ± 1.3	10.6 ± 1.3	10.4 ± 1.1	10.4 ± 0.9
SF-09-54	9.6 ± 0.9	10.0 ± 1.2	9.9 ± 1.2	9.7 ± 1.0	9.8 ± 0.9
SF-09-55	10.0 ± 0.9	10.4 ± 1.3	10.3 ± 1.3	10.1 ± 1.1	10.2 ± 0.9
SF-09-62	9.4 ± 0.9	9.9 ± 1.2	9.8 ± 1.2	9.5 ± 1.0	9.6 ± 0.9
SF-09-63	9.7 ± 1.0	10.1 ± 1.3	10.0 ± 1.3	9.8 ± 1.1	9.9 ± 1.0
SF-09-64	10.8 ± 1.1	11.4 ± 1.4	11.2 ± 1.4	11.0 ± 1.2	11.1 ± 1.1
SF-10-01	10.6 ± 1.0	11.2 ± 1.4	13.4 ± 1.3	10.9 ± 1.1	10.9 ± 1.0
Mean (all samples)*	10.0 ± 0.3	10.5 ± 0.4	10.4 ± 0.4	10.1± 0.3	10.2 ± 0.3
Mean (erratics)*	9.6 ± 0.4	10.0 ± 0.5	9.9 ± 0.5	9.6 ± 0.4	9.8 ± 0.4
Mean (bedrock)*	10.6 ± 0.4	11.1 ± 0.6	11.0 ± 0.5	10.7 ± 0.5	10.8 ± 0.4

*Error weighted mean and 1 s.d.

Table DR4 ^{10}Be and ^{26}Al ages from lower TIV referred to in this paper reproduced from Roberts et al. (2008) and recalculated using the regionally calibrated NE American production rate and Lal/Stone (Lal, 1990; Stone 2000) scaling. Original data and other parameters are documented in Roberts et al. (2008; Tables 1 and 2).

Sample	Latitude (°N)	Longitude (°W)	Elevation (m)	^{10}Be exposure age	^{26}Al exposure age
TI11	65.7005	38.1574	344	10.9 ± 0.9	12.4 ± 0.9
TI14	65.6960	38.1624	436	12.5 ± 1.1	13.6 ± 1.0
TI15	65.7054	38.1483	481	11.7 ± 0.9	--
TI17	65.7029	38.1799	78	12.6 ± 1.1	10.6 ± 1.6

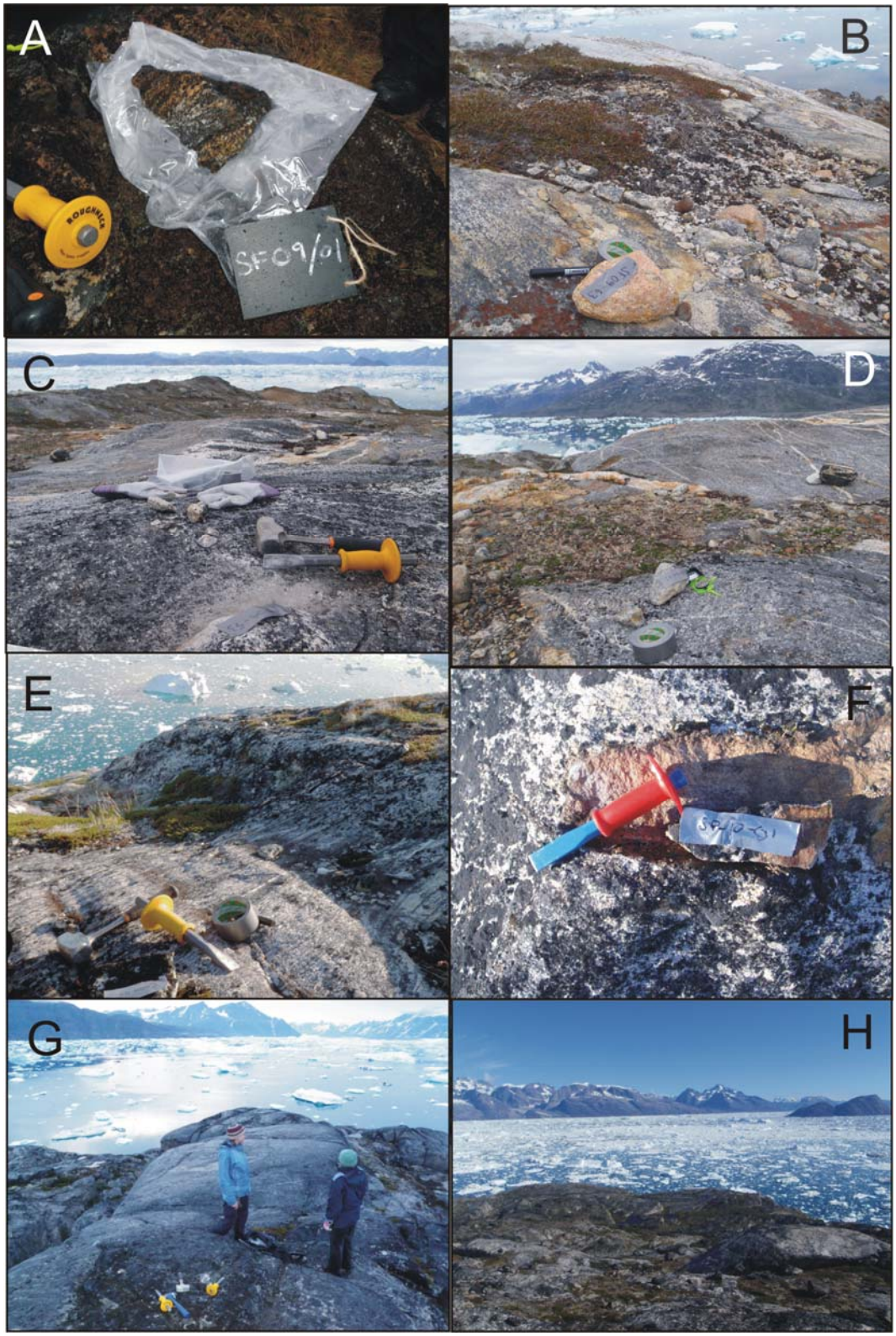

Figure DR1 Photographs of samples and sampling locations. (A) SF-09-01 bedrock sample. (B) SF-09-63 erratic sample resting on streamlined bedrock. (C) SF-09-53 bedrock sample and view up Sermilik Fjord looking northwest. (D) SF-09-54 erratic sample resting on streamlined bedrock. View of upper eastern side of Sermilik Fjord. (E) SF-09-29 erratic sample from southern flank of island at head of Sermilik Fjord. (F) SF-10-01 bedrock sample from head of Sermilik Fjord. (G) SF-09-03 bedrock sample from mouth of Helheimfjord. Background shows view over junction between Helheimfjord and Sermilik Fjord, looking northeast towards Fenris Glacier. (H) View from head of Sermilik Fjord looking south.

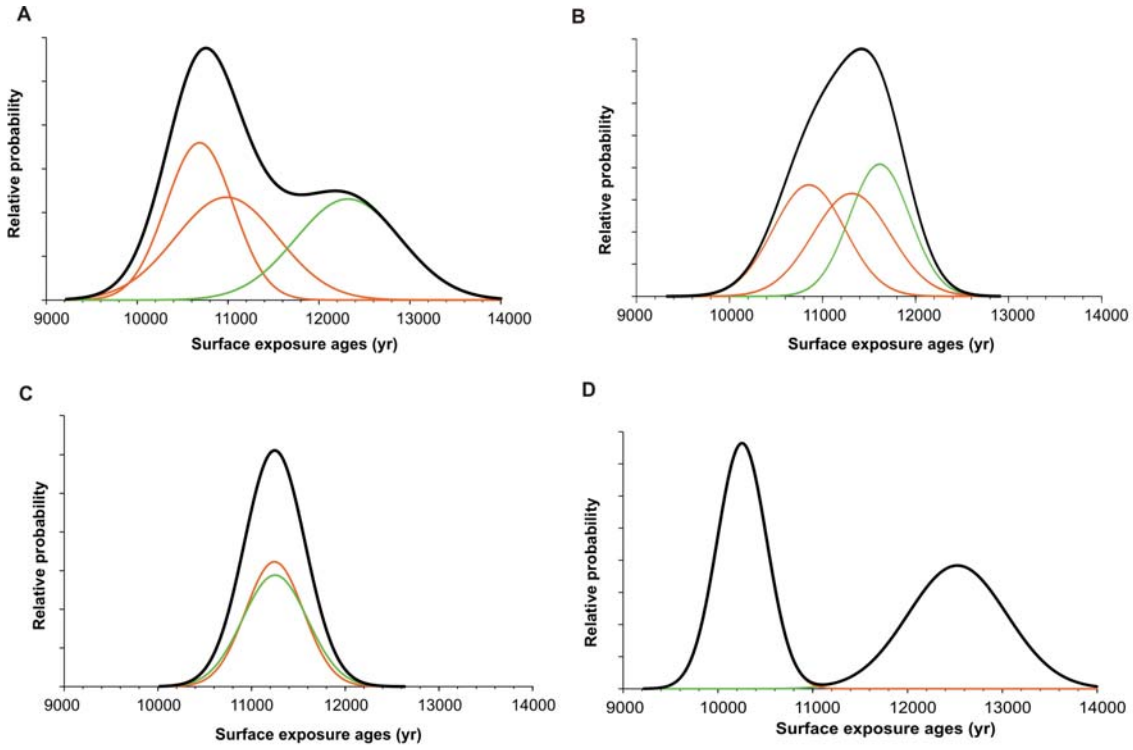

Figure DR2 Relative probability ('camel') plots of exposure ages of sites where there is more than one sample. Thin lines are Gaussian distributions of exposure ages with one sigma errors (internal uncertainties only). Bedrock age distributions are shown in green, erratic distributions in orange. Thick lines represent the sum of the individual distributions. (A) SF-09-62, SF-09-63, and SF-09-64, 27 km from Sermilik Fjord mouth. Although the three ages overlap within their error bounds, the erratic ages are clustered and the bedrock age is a distinct outlier. We interpret this as minor isotopic inheritance in the bedrock sample. (B). SF-09-53, SF-09-54, SF-09-55, 52 km from Sermilik Fjord mouth. All three ages overlap and are relatively tightly clustered. Any isotopic inheritance in the bedrock sample is very minor. (C) SF-09-29 and SF-09-30 from the island at the head of Sermilik Fjord are virtually indistinguishable. (D) SF-09-03 and SF-09-04 from the mouth of Helheimfjord are the only samples that do not overlap within error and their summed distribution lies directly on top of the individual distributions. We interpret the older bedrock age as reflecting isotopic inheritance in this sample and therefore regard the erratic age as more reliable at this site. Camel plots were generated in MATLAB after Balco (2001).

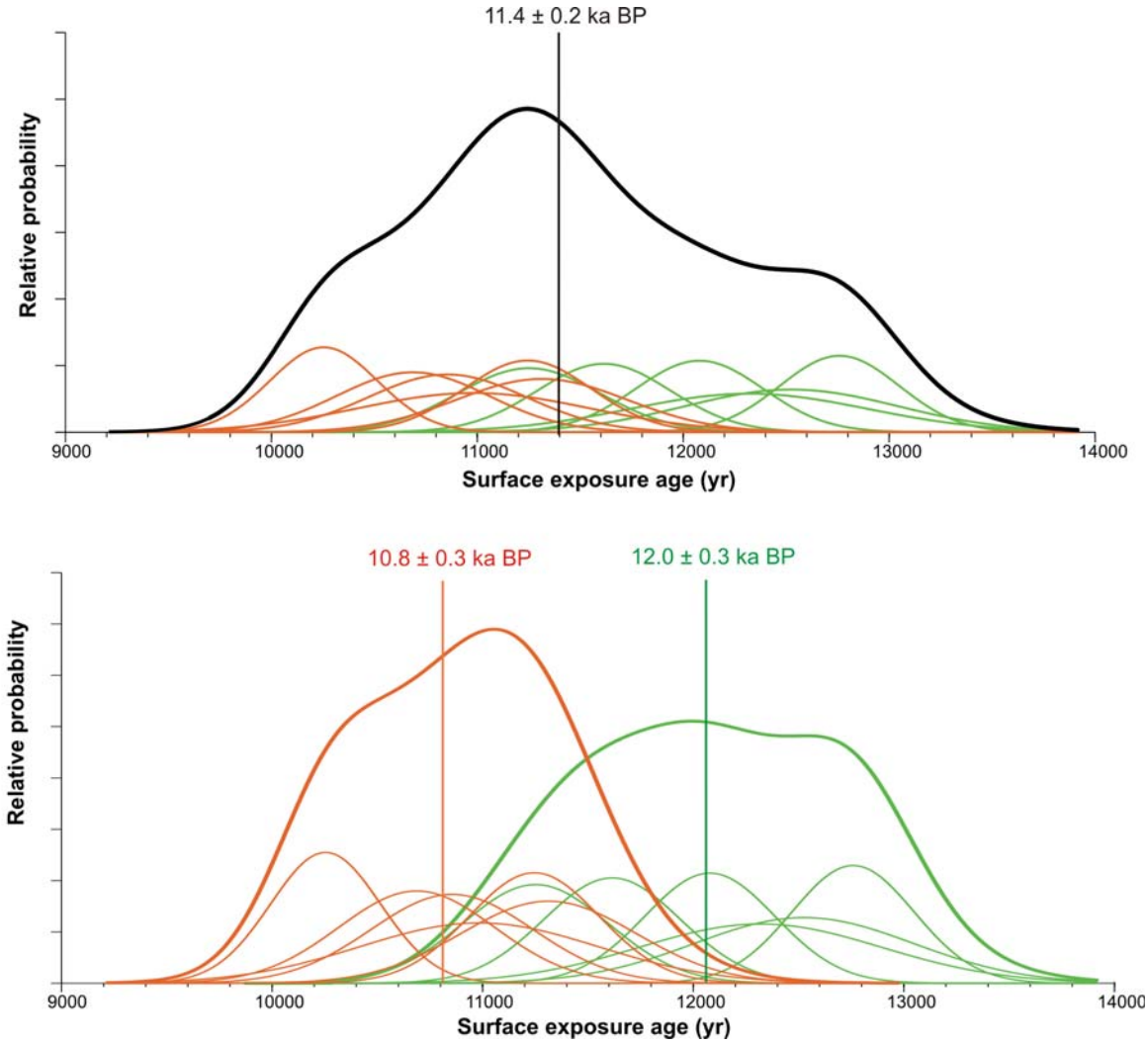

Figure DR3 Relative probability ('camel') plots of exposure ages of sites where there is more than one sample. Thin lines are Gaussian distributions of exposure ages with one sigma errors (internal uncertainties only). Bedrock age distributions are shown in green, erratic distributions in orange. Thick lines represent the sum of the individual distributions. The upper plot shows the summed total of all the ages from Sermilik Fjord. The lower plot shows the erratic and bedrock ages summed separately. Vertical lines show the weighted mean and standard deviation of each population (based on both internal and external uncertainties). Camel plots were generated in MATLAB after Balco (2001).

Supplementary References

André, M.-F., 2002, Rates of postglacial rock weathering on glacially scoured outcrops (Abisko-Riksgränsen area, 68°N): Geografiska Annaler, v. 84A, p. 139-150.

Balco, G. 2001. MATLAB code for camel diagrams [online]: http://depts.washington.edu/cosmolab/pubs/gb_pubs/camelplot.m, Last accessed: November 2011.

Balco, G., Briner, J., Finkel, R.C., Rayburn, J.A., Ridge, J.C., and Schaefer, J.M., 2009, Regional beryllium-10 production rate calibration for late-glacial northeastern North America: Quaternary Geochronology, v. 4, p. 93-107.

Balco, G., Stone, J.O., Lifton, N.A., and Dunai, T.J., 2008, A complete and easily accessible means of calculating surface exposure ages or erosion rates from ^{10}Be and ^{26}Al measurements: Quaternary Geochronology, v. 3, p. 174-195.

Briner, J.P., Bini, A.C., and Anderson, R.S., 2009, Rapid early Holocene retreat of a Laurentide outlet glacier through an Arctic fjord: Nature Geosci, v. 2, p. 496-499.

Briner, J.P., Young, N.E., Goehring, B.M., and Schaefer, J.M. In press. Constraining Holocene 10Be production rates in Greenland: Journal of Quaternary Science.

Chmeleff, J., von Blanckenburg, F., Kossert, K., and Jakob, D., 2010, Determination of the Be-10 half-life by multicollector ICP-MS and liquid scintillation counting: Nuclear Instruments & Methods in Physics Research Section B-Beam Interactions with Materials and Atoms, v. 268, p. 192-199.

Desilets, D., Zreda, M., and Prabu, T., 2006, Extended scaling factors for in situ cosmogenic nuclides: New measurements at low latitude: Earth and Planetary Science Letters, v. 246, p. 265-276.

Dunai, T.J., 2001, Influence of secular variation of the geomagnetic field on production rates of in situ produced cosmogenic nuclides: Earth and Planetary Science Letters, v. 193, p. 197-212.

Goehring, B.M., Lohne, Ø.S., Mangerud, J., Svendsen, J.I., Gyllencreutz, R., Schaefer, J., Finkel, R., In press. Late glacial and holocene ^{10}Be production rates for western Norway: Journal of Quaternary Science, doi: 10.1002/jqs.1517

Ivy-Ochs, S., 1996, The dating of rock surfaces using in situ produced ^{10}Be, ^{26}Al and ^{36}Cl, with examples from Antarctica and the Swiss Alps [PhD thesis]: Zurich, ETH.

Jakobsen, B.H., Fredskild, B., and Pedersen, J.B.T., 2008, Holocene changes in climate and vegetation in the Ammassalik area, East Greenland, recorded in lake sediments and soil profiles: Geografisk Tidsskrift-Danish Journal of Geography, v. 108, p. 21-50.

Kohl, C.P., and Nishiizumi, K., 1992, Chemical Isolation of Quartz for Measurement of Insitu-Produced Cosmogenic Nuclides: Geochimica Et Cosmochimica Acta, v. 56, p. 3583-3587.

Korschinek, G., Bergmaier, A., Faestermann, T., Gerstmann, U.C., Knie, K., Rugel, G., Wallner, A., Dillmann, I., Dollinger, G., von Gostomski, C.L., Kossert, K., Maiti, M., Poutivtsev, M., and Remmert, A., 2010, A new value for the half-life of Be-10 by Heavy-Ion Elastic Recoil Detection and liquid scintillation counting: Nuclear Instruments & Methods in Physics Research Section B-Beam Interactions with Materials and Atoms, v. 268, p. 187-191.

Lal, D., 1991, Cosmic-Ray Labelling of Erosion Surfaces – In situ Nuclide Production-Rates and Erosion Models: Earth and Planetary Science Letters, v. 104, p. 424-439.

Lifton, N.A., Bieber, J.W., Clem, J.M., Duldig, M.L., Evenson, P., Humble, J.E., and Pyle, R., 2005, Addressing solar modulation and long-term uncertainties in scaling secondary cosmic rays for in situ cosmogenic nuclide applications: Earth and Planetary Science Letters, v. 239, p. 140-161.

Long, A.J., Roberts, D.H., Simpson, M.J.R., Dawson, S., Milne, G.A., and Huybrechts, P., 2008, Late Weichselian relative sea-level changes and ice sheet history in southeast Greenland: Earth and Planetary Science Letters, v. 272, p. 8-18.

Nishiizumi, K., Imamura, M., Caffee, M.W., Southon, J.R., Finkel, R.C., and McAninch, J., 2007, Absolute calibration of Be-10 AMS standards: Nuclear Instruments & Methods in Physics Research Section B-Beam Interactions with Materials and Atoms, v. 258, p. 403-413.

Reimer, P.J., Baillie, M.G.L., Bard, E., Bayliss, A., Beck, J.W., Blackwell, P.G., Bronk Ramsey , C., Buck, C.E., Burr, G.S., Edwards, R.L., Friedrich, M., Grootes, P.M., Guilderson, T.P., Hajdas, I., Heaton, T.J., Hogg, A.G., Hughen, K.A., Kaiser, K.F., Kromer, B., McCormac, F.G., Manning, S.W., Reimer, R.W., Richards, D.A., Southon, J.R., Talamo, S., Turney, C.S.M., van der Plicht, J., and Weyhenmeyer, C.E. (2009) INTCAL 09 and MARINE09 radiocarbon age calibration curves, 0-50,000 years Cal BP. Radiocarbon: v. 51. p. 1111-1150.

Roberts, D.H., Long, A.J., Schnabel, C., Freeman, S., and Simpson, M.J.R., 2008, The deglacial history of southeast sector of the Greenland Ice Sheet during the Last Glacial Maximum: Quaternary Science Reviews, v. 27, p. 1505-1516.

Stone, J.O., 2000, Air pressure and cosmogenic isotope production: Journal of Geophysical Research-Solid Earth, v. 105, p. 23753-23759.

Stone, J. (2004), Extraction of Al and Be from quartz for isotopic analysis, [online]. (Available from: http://depts.washington.edu/cosmolab/chem.html).

Stuiver, M. and Reimer, P.J., 1993, Extended ^{14}C data base and revised CALIB 3.0 ^{14}C age calibration program, Radiocarbon, 35:215-230.

Xu, S., Dougans, A.B., Freeman, S.P.H.T., Schnabel, C., and Wilcken, K.M., 2010, Improved Be-10 and Al-26-AMS with a 5 MV spectrometer: Nuclear Instruments & Methods in Physics Research Section B-Beam Interactions with Materials and Atoms, v. 268, p. 736-738.

Young, N.E., Briner, J.P., Stewart, H.A.M., Axford, Y., Csatho, B., Rood, D.H., and Finkel, R.C., 2011, Response of Jakobshavn Isbrae Greenland, to Holocene climate change: Geology, v. 39, p. 131-134.